catalysts

MDPI

Review

Microporous Volumes from Nitrogen Adsorption at 77 K: When to Use a Different Standard Isotherm?

João Pires [1,*], Rafaela Fernandes [1], Moisés L. Pinto [2] and Mary Batista [1]

[1] CQE, Centro de Química Estrutural, Faculdade de Ciências, Universidade de Lisboa, 1749-016 Lisboa, Portugal; rafa_fernandes@outlook.pt (R.F.); mkbatista@fc.ul.pt (M.B.)
[2] CERENA, Departamento de Engenharia Química, Instituto Superior Técnico, Universidade de Lisboa, 1049-001 Lisboa, Portugal; moises.pinto@tecnico.ulisboa.pt
* Correspondence: jpsilva@ciencias.ulisboa.pt; Tel.: +351-217-500-903

Abstract: This work reviews the application of various standard isotherms to evaluate the micropore volume in a range of microporous materials. The selected materials have quite different surface chemistry, and are relevant due to their properties for adsorption and catalysis: zeolites, activated carbons, clay-based materials and MOFs. Some cases were analysed before and after being used as supports in the heterogenization of homogeneous catalysts. The discussion is centred, but not limited, to the three standard isotherms that are mostly employed in the literature (*t*-curve, non-porous carbon and non-porous hydroxylated silica) for the assessment of the micropore volume. For a given material the values of the micropore volumes from the different standard isotherms were compared, particularly against the values from the largely used *t*-curve. The cases where major discrepancies were found could normally be ascribed to samples that have a broad micropore size distribution.

Keywords: nitrogen-adsorption; standard-isotherm; microporosity

Citation: Pires, J.; Fernandes, R.; Pinto, M.L.; Batista, M. Microporous Volumes from Nitrogen Adsorption at 77 K: When to Use a Different Standard Isotherm? *Catalysts* **2021**, *11*, 1544. https://doi.org/10.3390/catal11121544

Academic Editors: Hamidreza Arandiyan and Gloria Berlier

Received: 18 November 2021
Accepted: 15 December 2021
Published: 18 December 2021

1. Introduction

As is well known, nitrogen adsorption at 77 K is the standard technique for the characterization of microporosity in nanoporous materials. This has been well established over the decades in fundamental text books [1–3] and IUPAC reports [4–6], although other gases were also proposed, for instance, argon [6] or carbon dioxide [7]. Even when a material also has meso and macropores (as defined by IUPAC [4]) alongside micropores, microporosity can strongly conditionate important properties. Examples of these properties are the adsorption/separation of gases and the catalytic activity [8] or the storage/release of small molecules for therapeutic applications [9]. Additionally, the precise determination of microporous volumes is critical in the experimental development of computationally predicted structures of new types of materials such as metal and covalent organic frameworks (MOFs and COFs) or porous polymer networks PPNs [10]. In this sense, is quite noteworthy that a relatively simple methodology for the evaluation of microporous volumes such as *t*-plots and a_s-plots which are, in their nature, empirical methods to analyse adsorption isotherms [2], remain widely used and continue to provide reliable results traversing decades of increasing computational and modelling development.

The basis of *t*-plots and a_s-plots is detailed in the literature [1–3] and their validity in various situations was discussed by several authors [11–13]. Briefly, to apply these methodologies the adsorption isotherm is replotted, keeping the adsorbed amounts (or volumes) on the material under study in ordinate and the abscissa is now a normalized unit [1] (*t* or a_s). The *t* or a_s values are obtained from the amount adsorbed in a given non-porous reference material (for the same relative pressure values) where a standard adsorption isotherm was obtained. The normalized unit *t* is the thickness of the adsorbed layers on the reference non-porous material, $t = (n/nm)\cdot\sigma$, where n is the amount adsorbed (at a given relative pressure), nm the amount adsorbed in the monolayer of the reference

material, and σ is the thickness of a single molecular layer, that is, the thickness of a monomolecular layer of, in the case of the present study, adsorbed nitrogen [1–3]. The *t*-plots are almost exclusively used when the standard isotherm corresponds to the *t*-curve for nitrogen adsorption, also sometimes referred to as "universal *t*-curve" [1,14–16] (Supplementary Materials). In the case of a_s-plots the normalized unit a_s is obtained by dividing the amount adsorbed n by $n_{0.4}$, that is, the amount adsorbed at the relative pressure of 0.4, $-a_s = (n/n_{0.4})$. Several standard isotherms that can be used to construct a_s-plots, on various types of non-porous reference materials such as silicas or carbons, but also for other adsorptives besides nitrogen, were published elsewhere [13,17–21].

The focus of the present work is on the evaluation of microporous volumes, although additional information could be obtained from *t*-plots and a_s-plots [1,2], namely the surface areas. Normally, for a material that has micro and mesopores these plots have the general shape illustrated in Figure 1. It is important to point out the different sections in these plots: section A reflects the adsorption in micropores, which is followed by a linear region in the plot (section B) and an upward deviation (section C) [1]. The latter can be absent if the material is exclusively microporous [1]. The microporous volume is obtained by the back extrapolation of the linear section in Figure 1 [2,6].

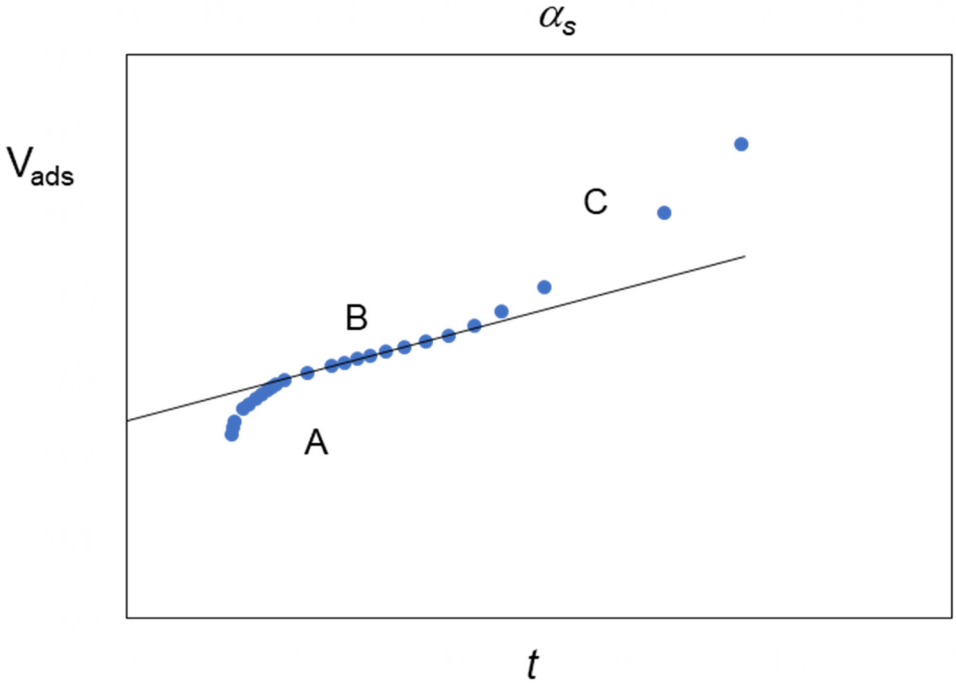

Figure 1. Schematic representation of *t* and a_s-plots.

For the accurate determination of the microporous volume, the correct choice of the standard isotherm is, therefore, important. In fact, the indication is that the appropriate standard isotherm must be determined on a non-porous solid having a surface chemistry of the same type as that of the studied adsorbent [2]. As mentioned, there are in the literature various standard isotherms for the adsorption of nitrogen at 77 K in several non-porous materials such as carbons, zeolites or clay-based materials. However, presently the variability of surfaces (and hence of surface chemistry) of adsorbents and catalysts is tremendous. In fact, if one thinks for instance of MOFs and related materials, the composition variability of these solids would render the attempt of using specific standard reference isotherms a formidable and virtually impossible task. Additionally, the case of the functionalization of the surface of porous materials with organic molecules, particularly regarding the heterogenization of homogeneous catalysts [22,23], producing new types of surfaces, is also relevant. In the present work, we critically review and discuss the effect of using various types of standard isotherms in the determination of the microporous volumes

from nitrogen adsorption data at 77 K in materials selected for their rather different surface chemistry, such as zeolites, activated carbons, clay-based materials and MOFs, some of them before and after being used as supports in the heterogenization of homogeneous catalysts.

2. Results and Discussion

The standard nitrogen isotherms at 77 K (all obtained in non-porous materials) considered in this work were: (i) the universal *t*-curve [24]; (ii) a carbon [25], (iii) a hydroxylated silica [1] and (iv) a char. The standard isotherms (i) to (iii) have been widely used in the literature. The use in this work of a char as standard reference material is because the microporous carbons studied here were prepared using this (non-porous) char as starting material, as discussed below.

Figure 2a presents the nitrogen adsorption isotherms at 77 K for the activated carbons C1, C2 and C3 (hereafter mentioned as carbons or carbon materials) prepared as described in Supplementary Materials, where the pore size distribution is also given. As per Figure 2a the isotherms for C1 and C2 are highly rectangular (Type I [6]), although for the latter some mesoporosity is also noticed, as indicated by the hysteresis cycle in C2. For the C3 sample, this rectangular character is much less pronounced as a consequence of a broader range of micropore sizes that may include small mesopores [6]. This is shown in the pore size distribution of C3 presented in Supplementary Materials. The *t*-plots and a_s-plots for samples C1 and C2 (Figure 3) show that for these samples, the microporous volumes (back-extrapolation of the straight lines) are almost independent of the standard isotherm that is used. In fact, (see Table 1) the microporous volumes vary at most by 2.7%. Furthermore, if we consider the difference between the values obtained by using the carbon, the hydroxylated silica and the char by one hand and the value obtained from the universal *t*-curve by the other hand (the Δ_{max} for *t* in Table 1), the value is even smaller.

In the case of the C3 sample, that is, the material with the broader distribution of pore sizes, the situation is much different since a strong effect of the nature of the standard isotherm is observed (Figure 3). In this case, the values of the micropore volume can vary up to 26.2% (Table 1) depending on the standard isotherm used, with the values from the *t*-curve and from the carbon standard material being the closer ones. The general observation for the studied carbon materials is that for the samples with highly rectangular isotherms, the influence of the standard isotherm is small, but this is not the case for the sample with a broad micropore distribution, that is, the less rectangular isotherm.

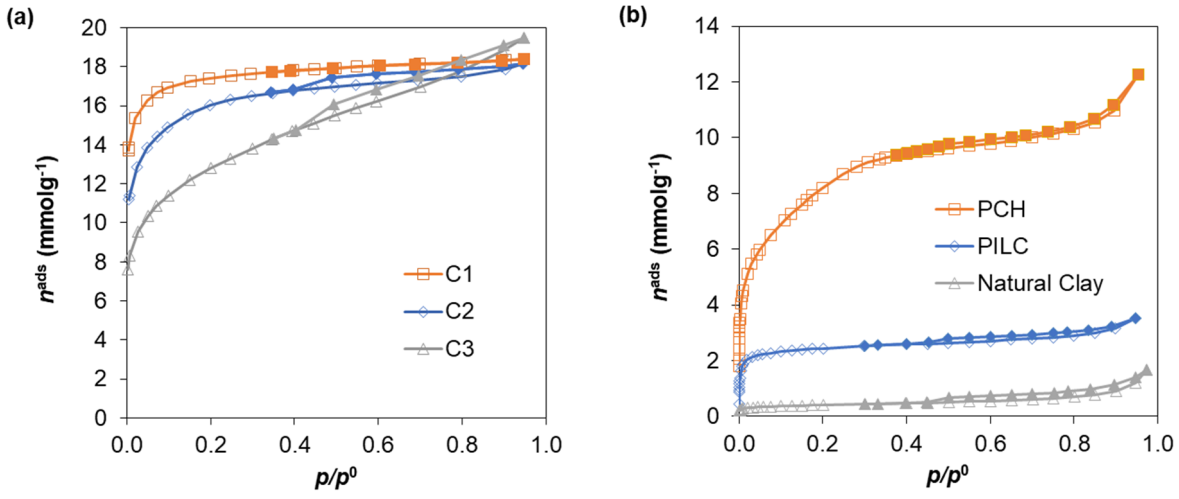

Figure 2. *Cont.*

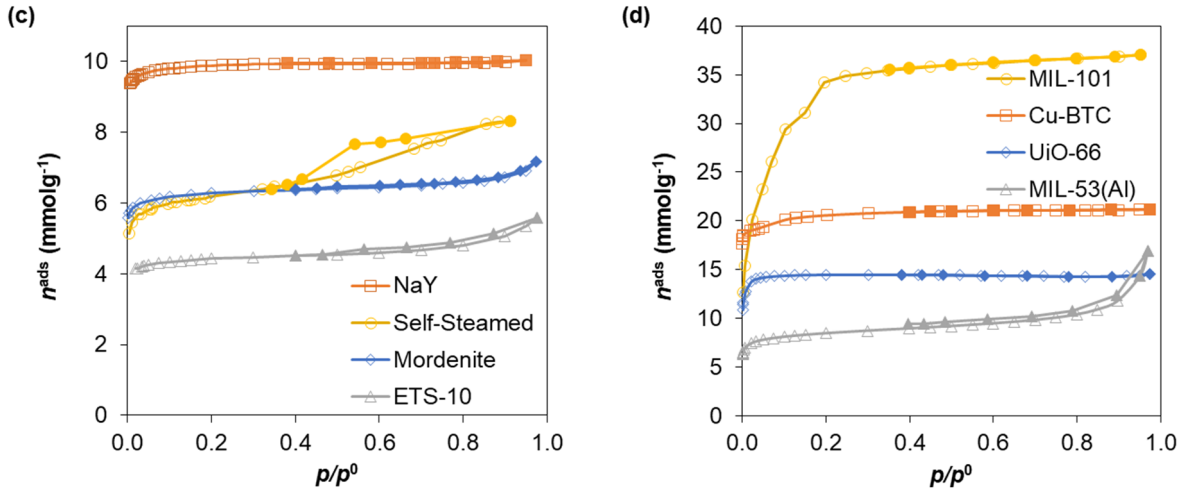

Figure 2. Nitrogen adsorption isotherms at 77 K (closed points for desorption) in the various types of materials studied in this work: (**a**) activated carbons; (**b**) clay-based materials; (**c**) zeolites and (**d**) MOFs. Data from [26–31].

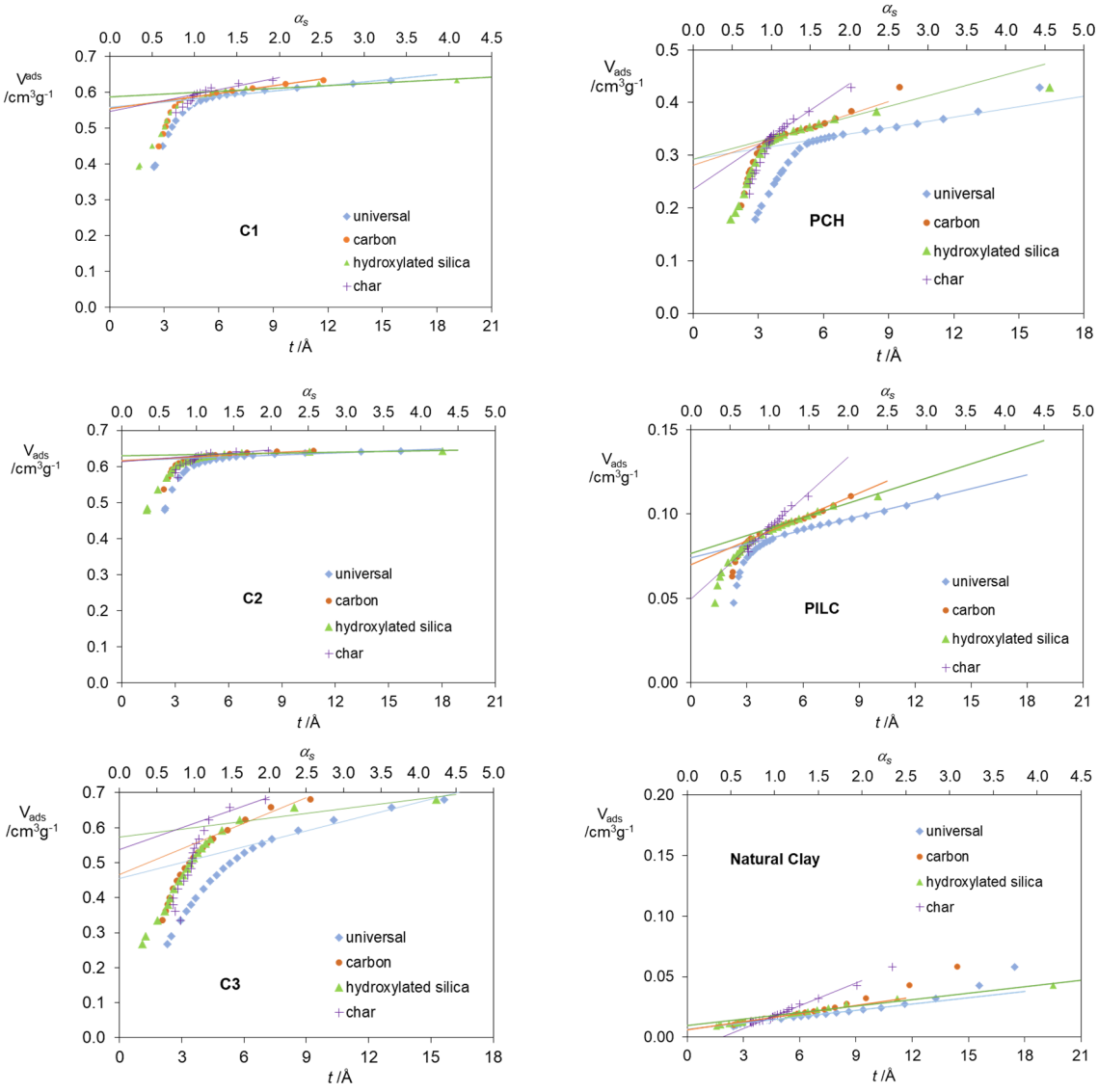

Figure 3. t and a_S-plots for the indicated materials using various standard isotherms.

Although the standard isotherm obtained in the char and, to a certain extent also for the standard carbon material, might not have an a priori relation with the surfaces of some of the examples of the materials mentioned in Figure 2, we keep these two standard isotherms for the sake of the discussion below.

The isotherms for the clay-based materials are given in Figure 2b. In this figure, the parent natural clay [26] was the starting material to prepare a pillared clay [32] with aluminium oxide pillars (PILC) [26] and a porous clay heterostructure (PCH) [33]. As expected, the natural clay has no relevant microporosity and the back extrapolations of all straight lines in Figure 3 for this material approach zero. In the case of the PILC and PCH (Figure 3), and according to the values of Table 1, if the char is included, the differences amongst the values can reach 35.1%. Nevertheless, the microporous volumes of the PILC and PCH samples obtained from the *t*-curve and the hydroxylated silica are very close (cf. Table 1).

The nitrogen adsorption isotherms in Figure 2c relate to four zeolites. One is the sodic form of Y zeolite (NaY) that has a cage structure with openings of 7.3 Å [34]. The "Self-Steamed" sample is a dealuminated form prepared from Y zeolite by a self-steaming process as described and characterized elsewhere [28]. As is well known, the dealumination of zeolites can improve their acid properties and thermal stability, hence improving the catalytic performance of the zeolite [35]. Besides, the steep initial section of the nitrogen isotherm, this sample also presents hysteresis because of the mesoporosity developed during the dealumination process [28] (mesopore size distribution in Supplementary Materials).

Two additional zeolites are included in Figure 2c, one is the Mordenite, which consists of a framework with channels that have openings of 6.7 Å [36], and the other is a titanosilicate (ETS-10) that has pores with openings of 6 × 8 Å and 6 Å [29]. Since all the isotherms in Figure 2c are very steep in the low-pressure region, as expected for materials with narrow distribution of small micropores, the *t*-plots and a_s-plots for the zeolites (Figure 4) gave microporous volumes that are rather independent of the standard isotherm used (see Table 1 also). This is even observed using the standard isotherm of the char. An exception is the titanosilicate ETS-10 where the maximum discrepancy (Table 1) can reach 15%, when using the standard isotherm for the hydroxylated silica.

Table 1. Microporous volumes determined from the nitrogen adsorption isotherm at 77 K using various standard isotherms in non-porous reference materials (Universal *t*-curve [24], Carbon [25], Hydroxylated silica [1] and a Char).

Standard Material	→	**Microporous Volume ($cm^3\ g^{-1}$)**				Δ_{max} (%) (a)	$\Delta_{max\ for\ t}$ (%) (b)
		Universal *t*-Curve	**Carbon**	**Hydroxylated Silica**	**Char**		
Carbon materials	C1	0.615	0.615	0.630	0.613	2.7	0.3
	C2	0.559	0.554	0.538	0.547	1.7	2.1
	C3	0.455	0.466	0.574	0.558	22.6	26.2
Clay materials	PCH	0.292	0.281	0.293	0.235	19.8	19.5
	PILC	0.074	0.07	0.077	0.05	35.1	32.4
	Clay	0.007	0.006	0.004	-	-	-
Zeolites	NaY	0.345	0.346	0.347	0.348	0.9	0.9
	Mordenite	0.213	0.211	0.216	0.206	4.6	3.3
	ETS-10	0.141	0.138	0.153	0.130	15.0	7.8
	Self-Steamed	0.163	0.159	0.155	0.161	4.9	4.9
MOFs	Cu-BTC	0.734	0.733	0.736	0.734	0.1	0.1
	UiO-66	0.505	0.505	0.503	0.504	0.4	0.4
	MIL-53(Al)	0.252	0.245	0.267	0.169	36.7	32.9
	MIL-101	1.212	1.220	1.248	1.23	2.9	−3.0

(a) Maximum difference between the microporous volumes irrespective of the standard isotherm. (b) Maximum difference for the microporous volume obtained using the universal *t*-curve.

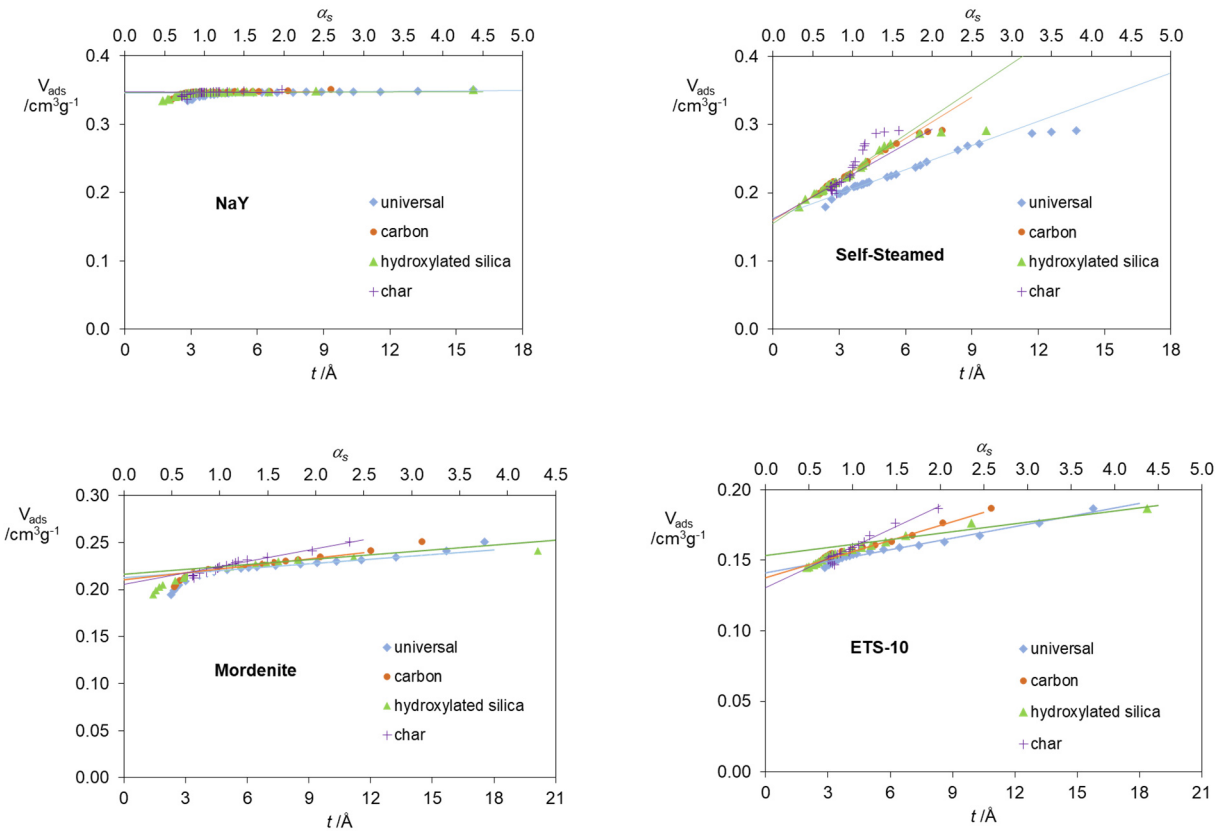

Figure 4. t and a_s-plots for the indicated materials using various standard isotherms.

For the MOF materials, the nitrogen adsorption isotherms at 77 K are presented in Figure 2d, namely: MIL-101 [30], UiO-66 [31] and Cu-BTC and MIL-53(Al) (the latter two isotherms were determined in this work). The MIL-101 used is a chromium(III) terephthalate MOF with a structure in cages of internal free diameters of 29 and 34 Å (that is, in the range of mesopores) accessible by openings of 12 Å and 14.5 × 16 Å [37]. UiO-66 is a zirconium MOF where 1,4-benzene-dicarboxylate is used as the organic linker [38]. The access to the internal tetrahedral and octahedral cages of UiO-66 is made by windows of 6 Å [38]. Cu-BTC is a copper-based MOF where the Cu(II) metal units are linked by benzene-1,3,5-tricarboxylate (BTC) linkers [39]. The main pores of Cu-BTC are of ca. 9 Å in diameter with side pockets with openings of 3.5 Å [40]. Concerning MIL-53(Al), its structure is formed by $AlO_4(OH)_2$ octahedra linked by 1,4-benzenedicarboxylate ligands [41]. The internal opening of the pores of MIL-53(Al) is 8.5 Å, but this material also has the particular feature that the pore openings can vary upon the adsorption-desorption of molecules in its structure, a feature that some authors classify as the "breathing" effect [41,42]. As can be seen from the t-plots and a_s-plots (Figure 5), the microporous volumes of the MOFs studied here (Table 1) are almost independent (within each MOF) of the standard isotherm used, inclusively, and somewhat unexpectedly, when the char is used as standard. The exception is for the MIL-53(Al) sample (Figure 5 and Table 1) for which the discrepancies can achieve 36.7%, although they decrease to 8% if the char is ruled out as standard material. If for Cu-BTC and UiO-66 this relative invariance of the micropore volumes with the type of standard isotherm could be anticipated, in light of the above results that showed that this is relatively common for high rectangular isotherms, the case of MIL-101 would be less predictable. In fact, for this material, the nitrogen isotherm is the least rectangular of those presented by the MOF materials (Figure 2d) but the structural regularity, that is, the uniformity of the pore dimensions, also appears to be key. In fact, MIL-101 clear presents a *plateau* above $p/p^0 = 0.4$ (Figure 2b) that corresponds to the saturation of the pores, which

will afterwards also produce a consistent plateau in the *t*-plot and a_s-plot leading to the same value of porous volume.

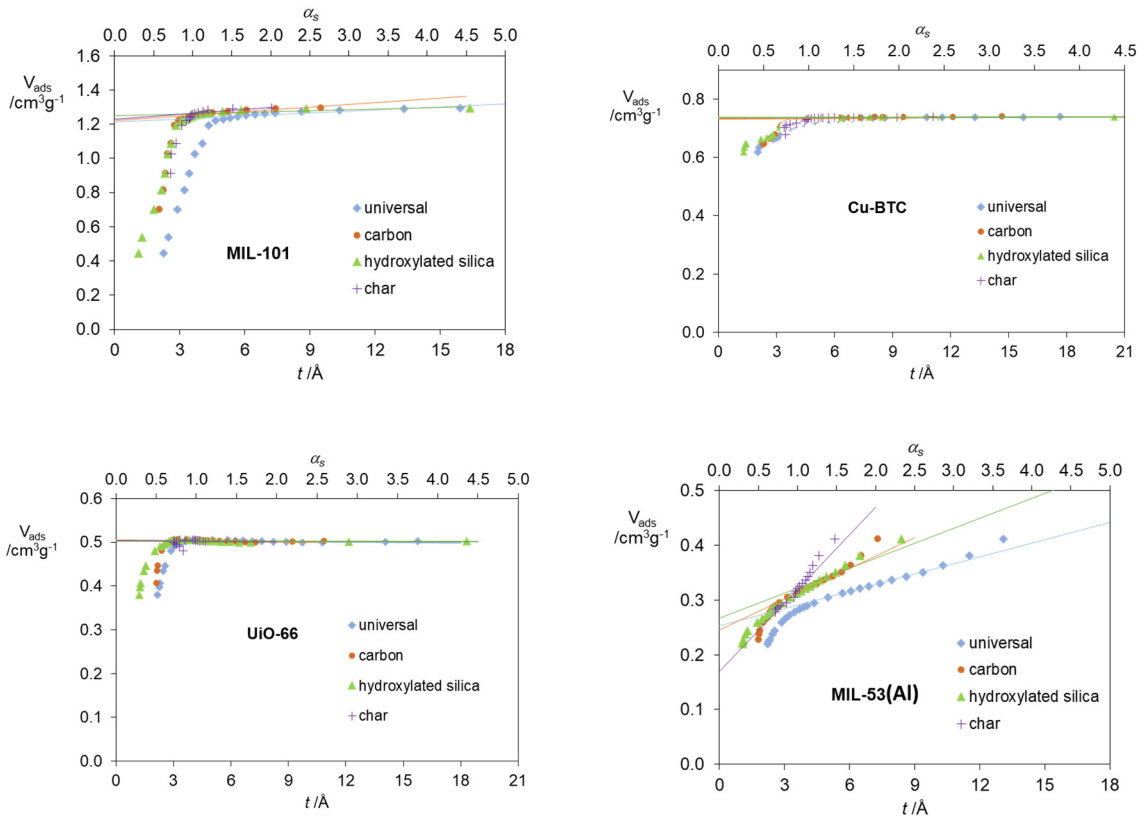

Figure 5. *t* and a_s-plots for the indicated materials using various standard isotherms.

In the case of the more regular materials (Zeolites and MOFs), an exercise can be made comparing the values in Table 1 with the values for the network-accessible geometric volume. These values can be estimated, for instance, through PoreBlazer [43] and are presented in Supplementary Materials. For the zeolites, the values agree for NaY and ETS-10, although for Mordenite the geometric values are higher, most probably due to limitations of the access of the nitrogen molecule to the small side pockets lateral to the main Mordenite channels in the real structure of this zeolite and/or other possible position of the cations not considered in the calculations. In the case of the MOFs materials, the values in Table 1 agree for Cu-BTC but some discrepancies were noticed for the other materials. In fact, the values for MIL-53(Al) are quite different, which can be related to the expandable nature of this MOF (i.e., the breathing effect between large and narrow pore configuration [41]) and the corresponding difficulty in having the most appropriate parameters that describe the structure of the material. The network-accessible geometric volume obtained for MIL-101 is higher than that reported in Table 1, pointing out that in the case of this MOF, where the pore openings are within the micropore dimensions but the internal dimensions of the cages are already in the range of the mesopores, the results obtained by *t*-plots and a_s-plots can provide values below the expected ones.

In the following part of the text, the effect of using different standard isotherms to evaluate microporous volumes is discussed for supported and/or heterogenized catalysts [23]. In fact, the heterogeneization of homogeneous catalysts is an important strategy to obtain supported catalysts that keep the homogeneous catalytic sites with the benefits of easy separation and, most important, recycling [22,23]. While homogeneous catalysis, in theory, has advantages over heterogeneous catalysis due to, for instance, less diffusional constraints of the reactants and products, in heterogeneous catalysis the catalyst can be easily recovered using filtration or extraction techniques [22]. Upon heterogenization, often

preceded by a step of surface functionalization to anchor the homogeneous catalyst, usually a metal complex [22,23], the porosity and the nature of the surface of the supporting material is changed. The nitrogen adsorption isotherms at 77 K in examples of heterogenized materials, using various types of supports, are given in Figure 6a–c.

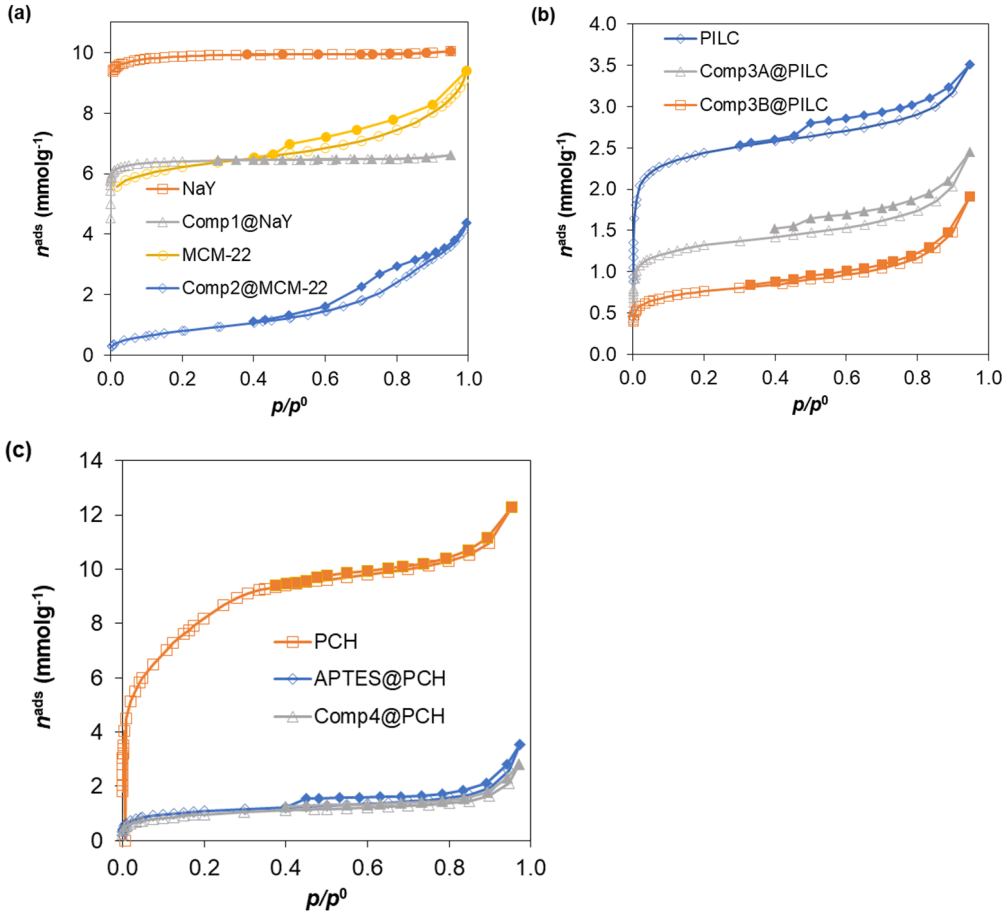

Figure 6. Nitrogen adsorption isotherms at 77 K (closed points for desorption) in parent materials and in materials modified by catalyst heterogenization: (**a**) zeolites; (**b**) pillared-clays; (**c**) porous clays heterostructures. Data from [26–28,44,45].

In the case of Figure 6a, the inclusion of the complex Comp1 (structure in Supplementary Materials) in the NaY zeolite, decreases the adsorption capacity but maintains the Type I [6] character of the adsorption isotherm. In this way, and although the surface of the parent NaY zeolite was modified by the presence of the complex Comp1, the microporous volumes determined using the carbon or the hydroxylated silica (Figure 7 and Table 2) only differ, at the maximum, by 3.6% from the values determined using the *t*-curve.

In the case of the MCM-22 zeolite (Figure 6a), the example included a copper complex Comp2 (structure in Supplementary Materials) which is active for instance in cyclopropanation of styrene [40]. The MCM-22 zeolite has a structure with two independent internal micropore systems. One is composed of cylindrical cages (7.1 Å × 18.2 Å) interconnected by 10 membered-ring windows (4.0 × 5.5 Å) [41]. A second pore system is constituted by sinusoidal channels (4.1 × 5.1 Å). A particularity of this zeolite is that the external surface of the crystals is covered by half cavities (7.1 × 7 Å) [41]. Upon the immobilization of Comp2, the MCM-22 zeolite has the microporosity completely blocked, as illustrated in Figure 7 (and Table 2). Nevertheless, due to its particular structure, namely the mentioned cavities in the external surface, the material still has catalytic activity for the reaction of cyclopropanation of styrene with ethyldiazoacetate [40].

Table 2. Microporous volumes determined from the nitrogen adsorption isotherm at 77 K using various standard isotherms in non-porous reference materials (Universal *t*-curve [24], Carbon [25] and Hydroxylated silica [1]).

Standard Material	→	Microporous Volume ($cm^3\ g^{-1}$)			$\Delta_{for\ t}$ (%) (Carbon) (a)	$\Delta_{for\ t}$ (%) (Hyd. Silica) (b)
		Universal *t*-Curve	Carbon	Hydroxylated Silica		
Zeolites	NaY	0.345	0.346	0.347	0.3	0.6
	Comp1@NaY	0.224	0.218	0.216	2.7	3.6
	MCM-22	0.188	0.178	0.173	5.3	8.0
	Comp2@MCM-22	0	0	0	0	0
PILCs	PILC	0.074	0.07	0.077	5.4	4.1
	Comp3a@PILC	0.034	0.032	0.032	5.9	5.9
	Comp3b@PILC	0.016	0.015	0.014	6.3	12.5
PCHs	PCH	0.292	0.281	0.293	3.8	0.3
	APTES@PCH	0.027	0.026	0.024	3.7	11.1
	Comp4@PCH	0.028	0.028	0.026	0.0	10.7

(a) Difference between the value using the universal *t*-curve and using the non-porous carbon as standard. (b) Difference between the value using the universal *t*-curve and using the non-porous hydroxylated silica as standard.

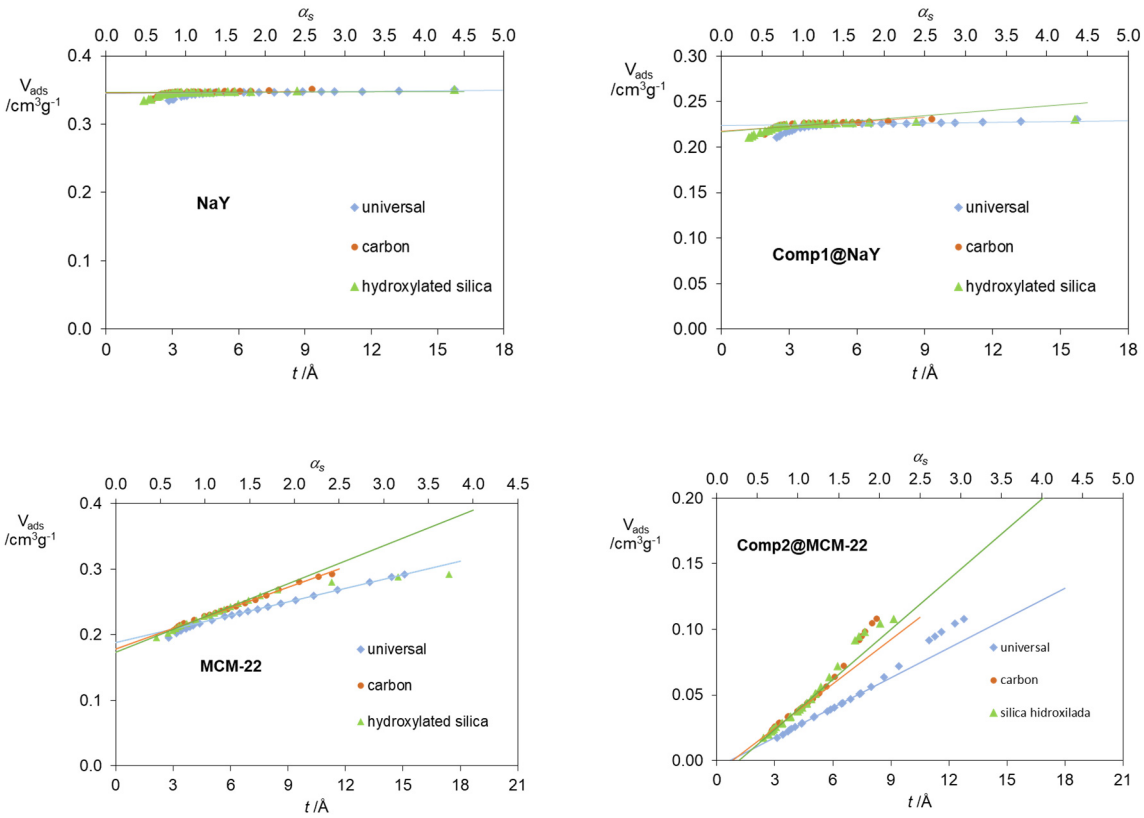

Figure 7. *t* and a_s-plots for the indicated materials using various standard isotherms.

Figure 6b exemplifies a case where a natural clay was used to immobilize a manganese(III)-salen complex (Comp3)—structure in Supplementary Materials S4—by two different methodologies [26], hence the samples Comp3a@PILC and Comp3b@PILC. As usually occurs upon the heterogenization by the immobilization of bulky metal complexes, the adsorption capacity is reduced, and the effect of the standard isotherm increases as the microporous volume decreases (Table 2).

The oxovanadium(IV) acetylacetonate—Comp4—(structure in Supplementary Materials S4) is an efficient homogeneous catalyst for the epoxidation reaction of allylic alcohols, presenting high activity, stereo- and regioselectivity [46]. This oxovanadium complex

was immobilized in various solid supports including in a porous clay heterostructure (PCH), as described elsewhere [27]. To ensure the efficient anchoring of the complex, the covalent immobilization was done through the first step of functionalisation of the surface of the material with 3-aminopropyltriethoxysilane (APTES). The nitrogen adsorption isotherms [27] in Figure 6c show an accentuated decrease in the adsorption capacity upon the functionalisation step with APTES. The microporous volumes from the various standard isotherms (Figure 8) are much similar for the parent PCH material than for the modified samples. Additionally, in the latter, the difference between the values from the *t*-curve and the carbon reference material are lower than those between the *t*-curve and the hydroxylated silica.

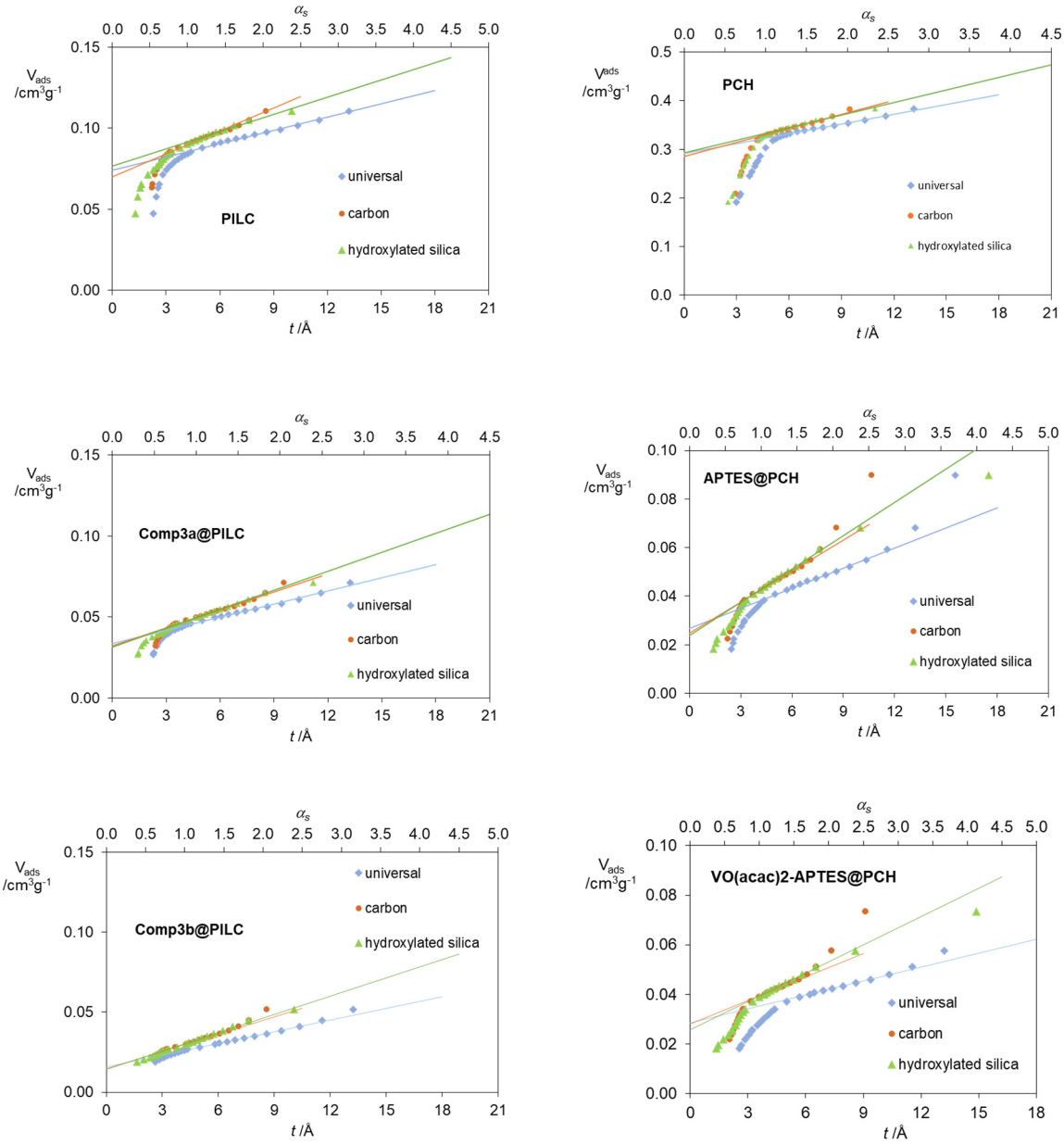

Figure 8. *t* and a_S-plots for the indicated materials using various standard isotherms.

3. Materials and Methods

The preparation of the char, and the activated carbons C1 and C2 obtained from this char, are described in Supplementary Materials. The standard isotherms (ii) to (iv) were used in the form of a_S-plots and the mathematical expressions for all the standard isotherms

used are given in Supplementary Materials. The N_2 adsorption isotherms at 77 K in the char and in the activated carbons C1, C2 and C3 were obtained in automatic equipment (Quantachrome mod. NOVA 2200e, Boynton. Beach, FL, USA). Before experiments, the samples (~100 mg) were outgassed overnight at 120 °C under a vacuum better than 10^{-2} Pa. The N_2 isotherm for the zeolite Mordenite was obtained in a similar way, but the outgassing was for 3 hours at 300 °C. In the t or a_s-plots, the amounts adsorbed are expressed in terms of liquid volume, by using the value of 0.809 g·cm^{-3} for the density of nitrogen at 77 K [2] to convert the units from mmog^{-1}. In the case of the MOFs Cu-BTC and MIL-53(Al), these were from Aldrich, Lisboa, Portugal and the samples were outgassed overnight at 120 °C under a vacuum better than 10^{-2} Pa before measurements. All the other results of the N_2 adsorption isotherms at 77 K discussed in this work were obtained from data previously published in the literature, as clearly indicated in the captions of Figures 2 and 6, as well as in the main text.

4. Conclusions

The effect of different standard isotherms in the determination of the microporous volumes from the nitrogen adsorption isotherm at 77 K, using standard isotherms in non-porous reference materials was reviewed for samples representative of various types of microporous materials, such as zeolites, clay-based materials, activated carbons and MOFs. One characteristic of the nitrogen isotherm that is more influential in this type of analysis is the rectangular (or Type I [6]) character. In fact, when, as a result of a less uniform distribution of micropore sizes, the Type I character of the nitrogen isotherm is less pronounced, the dependence of the values of the micropore volumes on the type of standard isotherm increases. Trends in the values of the micropore volumes (Tables 1 and 2) might not be easy to extract. Nevertheless, and considering the three most employed standard isotherms in the literature (t-curve [24], carbon [25] and hydroxylated silica [1]), the microporous volumes using the standard isotherm for the hydroxylated silica were the highest for 58% of the materials studied in this work. Additionally, and considering all the studied materials, the average of the differences between the values of the microporous volumes obtained from the t-curve and the curves for the carbon or the hydroxylated silica reference materials were 2.4 and 5.3%, respectively. In this way, for materials with narrow micropore size distribution, the "universal" t-curve [24] was showed to be adequate. In the case of materials that present a broad micropore size distribution, the uncertainties in the micropore volume determination appears to be more related to the limitations of the methodology than with the choice of the standard isotherm. For materials such as certain MOFs, which present structures with an expandable nature (i.e., the breathing effect), the conclusions were unclear.

Supplementary Materials: The following are available online at https://www.mdpi.com/article/10.3390/catal11121544/s1, Supplementary S1: Method for the preparation of the char and the activated carbons; Supplementary S2: Mathematical expressions for the various standard isotherms; Table S1: Coefficients of the polynomial equations that relate a_s and the relative pressure (p/p^0) for the standard isotherms on the hydroxylated silica, the carbon and the char; Supplementary S3: Pore size distributions; Figure S1: Pore size distributions for the carbon materials (C1, C2 and C3) and for the dealuminated Y zeolite (Self Steamed); Supplementary S4: Structures of the metallic complexes supported in different materials, Supplementary S5. Network-accessible geometric volume; Table S2: Network-accessible geometric volume (in cm^3 g^{-1}) obtained with PoreBlazer for the zeolites and MOFs studied in this work.

Author Contributions: Conceptualization, J.P. and M.B.; methodology, J.P., M.L.P. and M.B.; software, J.P., R.F. and M.L.P.; validation, J.P. and M.L.P.; formal analysis, J.P. and M.L.P.; investigation J.P., R.F., M.L.P. and M.B.; resources, J.P. and M.L.P.; writing—original draft preparation, J.P., R.F. and M.B.; writing—review and editing, J.P., M.L.P. and M.B.; supervision, J.P. and M.B.; funding acquisition, J.P. and M.L.P. All authors have read and agreed to the published version of the manuscript.

Funding: This research was funded by Fundação para a Ciência e a Tecnologia (FCT) in the scope of the projects UIDB/00100/2020 (CQE), UIDB/04028/2020 (CERENA). MB acknowledges for FCT-Investigator contract-DL57.

Conflicts of Interest: The authors declare that they have no known competing financial interests or personal relationships that could influence the work reported in this paper.

References

1. Gregg, S.J.; Sing, K.S.W. *Adsorption, Surface Area and Porosity*, 2nd ed.; Academic Press: Cambridge, MA, USA, 1982.
2. Rouquerol, F.; Rouquerol, J.; Sing, K.S.W.; Llewellyn, P.; Maurin, G. *Adsorption by Powders and Porous Solids Principles, Methodology and Applications*, 2nd ed.; Elsevier B.V.: Amsterdam, The Netherlands, 2014.
3. Marsh, H.; Rodríguez-Reinoso, F. Chapter 4—Characterization of Activated Carbon. In *Activated Carbon*; Marsh, H., Rodríguez-Reinoso, F., Eds.; Elsevier Science Ltd.: Oxford, UK, 2006; pp. 143–242. ISBN 978-0-08-044463-5.
4. Sing, K.S.W. Reporting physisorption data for gas/solid systems with special reference to the determination of surface area and porosity (Recommendations 1984). *Pure Appl. Chem.* **1985**, *57*, 603–619. [CrossRef]
5. Rouquerol, J.; Avnir, D.; Fairbridge, C.W.; Everett, D.H.; Haynes, J.H.; Pernicone, N.; Ramsay, J.D.F.; Sing, K.S.W.; Unger, K.K. Recomendations for the characterization of porous solids. *Pure Appl. Chem.* **1994**, *66*, 1739–1758. [CrossRef]
6. Thommes, M.; Kaneko, K.; Neimark, A.V.; Olivier, J.P.; Rodriguez-Reinoso, F.; Rouquerol, J.; Sing, K.S.W. Physisorption of gases, with special reference to the evaluation of surface area and pore size distribution (IUPAC Technical Report). *Pure Appl. Chem.* **2015**, *87*, 1051–1069. [CrossRef]
7. Silvestre-Albero, J.; Silvestre-Albero, A.; Rodríguez-Reinoso, F.; Thommes, M. Physical characterization of activated carbons with narrow microporosity by nitrogen (77.4K), carbon dioxide (273K) and argon (87.3K) adsorption in combination with immersion calorimetry. *Carbon* **2012**, *50*, 3128–3133. [CrossRef]
8. Kulprathipanja, S. *Zeolites in Industrial Separation and Catalysis*; Wiley-Vch: Weinheim, Germany, 2010.
9. McKinlay, A.C.; Morris, R.E.; Horcajada, P.; Férey, G.; Gref, R.; Couvreur, P.; Serre, C. BioMOFs: Metal–Organic Frameworks for Biological and Medical Applications. *Angew. Chem. Int. Ed.* **2010**, *49*, 6260–6266. [CrossRef]
10. Ongari, D.; Boyd, P.G.; Barthel, S.; Witman, M.; Haranczyk, M.; Smit, B. Accurate Characterization of the Pore Volume in Microporous Crystalline Materials. *Langmuir* **2017**, *33*, 14529–14538. [CrossRef]
11. Galarneau, A.; Villemot, F.; Rodriguez, J.; Fajula, F.; Coasne, B. Validity of the *t*-plot Method to Assess Microporosity in Hierarchical Micro/Mesoporous Materials. *Langmuir* **2014**, *30*, 13266–13274. [CrossRef] [PubMed]
12. Villemot, F.; Galarneau, A.; Coasne, B. Adsorption-based characterization of hierarchical metal–organic frameworks. *Adsorption* **2014**, *20*, 349–357. [CrossRef]
13. Villarroel-Rocha, J.; Barrera, D.; Blanco, A.A.G.; Jalil, M.E.R.; Sapag, K. Importance of the alpha(s)-plot Method in the Characterization of Nanoporous Materials. *Adsorpt. Sci. Technol.* **2013**, *31*, 165–183. [CrossRef]
14. Harkins, W.D.; Jura, G. Surfaces of Solids. XIII. A Vapor Adsorption Method for the Determination of the Area of a Solid without the Assumption of a Molecular Area, and the Areas Occupied by Nitrogen and Other Molecules on the Surface of a Solid. *J. Am. Chem. Soc.* **1944**, *66*, 1366–1373. [CrossRef]
15. Lippens, B.C.; de Boer, J.H. Studies on pore systems in catalysts III. Pore-size distribution curves in aluminum oxide systems. *J. Catal.* **1964**, *3*, 44–49. [CrossRef]
16. Lippens, B.C.; de Boer, J.H. Studies on pore systems in catalysts: V. The t method. *J. Catal.* **1965**, *4*, 319–323. [CrossRef]
17. Carrott, P.J.M.; Ribeiro Carrott, M.M.L.; Cansado, I.P.P. Reference data for the adsorption of dichloromethane on carbon materials. *Carbon* **2001**, *39*, 465–472. [CrossRef]
18. Carrott, P.J.M.; Sing, K.S.W. Multilayer adsorption of nitogen and alkanes by non-porous carbons and silicas. *Pure Appl. Chem.* **1989**, *61*, 1835–1840. [CrossRef]
19. Pires, J.; De Carvalho, M.B.; Carvalho, A.P. Aluminum-pillared clays: Decomposition of the intercalating species and textural properties. *Zeolites* **1997**, *19*, 107–113. [CrossRef]
20. Gardner, L.; Kruk, M.; Jaroniec, M. Reference Data for Argon Adsorption on Graphitized and Nongraphitized Carbon Blacks. *J. Phys. Chem. B* **2001**, *105*, 12516–12523. [CrossRef]
21. Bhambhani, M.R.; Cutting, P.A.; Sing, K.S.W.; Turk, D.H. Analysis of nitrogen adsorption isotherms on porous and nonporous silicas by the BET and αs methods. *J. Colloid Interface Sci.* **1972**, *38*, 109–117. [CrossRef]
22. Trindade, A.F.; Gois, P.M.P.; Afonso, C.A.M. Recyclable Stereoselective Catalysts. *Chem. Rev.* **2009**, *109*, 418–514. [CrossRef] [PubMed]
23. Barbaro, P.; Liguori, F. *Heterogenized Homogeneous Catalysts for Fine Chemicals Production*; Springer: Dordrecht, The Netherlands, 2010.
24. de Boer, J.H.; Lippens, B.C.; Linsen, B.G.; Broekhoff, J.C.P.; van den Heuvel, A.; Osinga, T.J. The t-curve of multimolecular N_2-adsorption. *J. Colloid Interface Sci.* **1966**, *21*, 405–414. [CrossRef]
25. Rodriguez-Reinoso, F.; Martin-Martinez, J.M.; Prado-Burguete, C.; McEnaney, B. A standard adsorption isotherm for the characterization of activated carbons. *J. Phys. Chem.* **1987**, *91*, 515–516. [CrossRef]

26. Cardoso, B.; Pires, J.; Carvalho, A.P.; Carvalho, M.B.; Kuźniarska-Biernacka, I.; Silva, A.R.; Freire, C.; de Castro, B. Catalytic Properties of a MnIII-Salen Complex Immobilised in a Pillared Clay by Simultaneous Pillaring/Encapsulation Procedures. *Eur. J. Inorg. Chem.* **2005**, *2005*, 837–844. [CrossRef]
27. Pereira, C.; Biernacki, K.; Rebelo, S.L.H.; Magalh?es, A.L.; Carvalho, A.P.; Pires, J.; Freire, C. Designing heterogeneous oxovanadium and copper acetylacetonate catalysts: Effect of covalent immobilisation in epoxidation and aziridination reactions. *J. Mol. Catal. A Chem.* **2009**, *312*, 53–64. [CrossRef]
28. Pires, J.; Carvalho, A.; Pinto, M.; Rocha, J. Characterization of Y zeolites dealuminated by solid-state reaction with ammonium hexafluorosilicate. *J. Porous Mater.* **2006**, *13*, 107–114. [CrossRef]
29. Pinto, M.L.; Fernandes, A.C.; Antunes, F.; Pires, J.; Rocha, J. Storage and delivery of nitric oxide by microporous titanosilicate ETS-10 and Al and Ga substituted analogues. *Microporous Mesoporous Mater.* **2016**, *229*, 83–89. [CrossRef]
30. Granadeiro, C.M.; Silva, P.; Saini, V.K.; Paz, F.A.A.; Pires, J.; Cunha-Silva, L.; Balula, S.S. Novel heterogeneous catalysts based on lanthanopolyoxometalates supported on MIL-101(Cr). *Catal. Today* **2013**, *218–219*, 35–42. [CrossRef]
31. Pinto, M.L.; Dias, S.; Pires, J. Composite MOF foams: The example of UiO-66/polyurethane. *ACS Appl. Mater. Interfaces* **2013**, *5*, 2360–2363. [CrossRef]
32. Schoonheydt, R.A.; Pinnavaia, T.; Lagaly, G.; Gangas, N. Pillared clays and pillared layered solids—Technical Report. *PURE Appl. Chem.* **1999**, *71*, 2367–2371. [CrossRef]
33. Kuźniarska-Biernacka, I.; Pereira, C.; Carvalho, A.P.; Pires, J.; Freire, C. Epoxidation of olefins catalyzed by manganese (III) salen complexes grafted to porous heterostructured clays. *Appl. Clay Sci.* **2011**, *53*, 195–203. [CrossRef]
34. Database of Zeolite Structures. Available online: https://europe.iza-structure.org/IZA-SC/framework.php?STC=FAU (accessed on 27 September 2021).
35. Gola, A.; Rebours, B.; Milazzo, E.; Lynch, J.; Benazzi, E.; Lacombe, S.; Delevoye, L.; Fernandez, C. Effect of leaching agent in the dealumination of stabilized Y zeolites. *Microporous Mesoporous Mater.* **2000**, *40*, 73–83. [CrossRef]
36. Database of Zeolite Structures. Available online: https://europe.iza-structure.org/IZA-SC/framework.php?STC=MOR (accessed on 15 November 2021).
37. Ferey, G.; Mellot-Draznieks, C.; Serre, C.; Millange, F.; Dutour, J.; Surble, S.; Margiolaki, I. A chromium terephthalate-based solid with unusually large pore volumes and surface area. *Science* **2005**, *309*, 2040–2042. [CrossRef]
38. Cavka, J.H.; Jakobsen, S.; Olsbye, U.; Guillou, N.; Lamberti, C.; Bordiga, S.; Lillerud, K.P. A New Zirconium Inorganic Building Brick Forming Metal Organic Frameworks with Exceptional Stability. *J. Am. Chem. Soc.* **2008**, *130*, 13850–13851. [CrossRef] [PubMed]
39. Chui, S.S.Y.; Lo, S.M.F.; Charmant, J.P.H.; Orpen, A.G.; Williams, I.D. A chemically functionalizable nanoporous material $[Cu_3(TMA)_2(H2O)_3]_n$. *Science* **1999**, *283*, 1148–1150. [CrossRef] [PubMed]
40. Vishnyakov, A.; Ravikovitch, P.I.; Neimark, A.V.; Bulow, M. Nanopore structure and sorption properties of Cu-BTC metal-organic framework. *Abstr. Pap. Am. Chem. Soc.* **2003**, *3*, 713–718. [CrossRef]
41. Loiseau, T.; Serre, C.; Huguenard, C.; Fink, G.; Taulelle, F.; Henry, M.; Bataille, T.; Férey, G. A Rationale for the Large Breathing of the Porous Aluminum Terephthalate (MIL-53) Upon Hydration. *Chem. A Eur. J.* **2004**, *10*, 1373–1382. [CrossRef]
42. Moreira, M.A.; Santos, J.C.; Ferreira, A.F.P.; Müller, U.; Trukhan, N.; Loureiro, J.M.; Rodrigues, A.E. Selective Liquid Phase Adsorption and Separation of ortho-Xylene with the Microporous MIL-53(Al). *Sep. Sci. Technol.* **2011**, *46*, 1995–2003. [CrossRef]
43. Sarkisov, L.; Harrison, A. Computational structure characterisation tools in application to ordered and disordered porous materials. *Mol. Simul.* **2011**, *37*, 1248–1257. [CrossRef]
44. Costa, F.; Fonseca, A.M.; Neves, I.C.; Carvalho, A.P.; Pires, J. Immobilization of hybride tungsten complex in microporous structures. In *Materials Science Forum*; Trans Tech Publications Ltd.: Freienbach, Switzerland, 2006; Volumes 514–516, ISBN 9780878494026.
45. Silva, A.R.; Guimarães, V.; Carneiro, L.; Nunes, N.; Borges, S.; Pires, J.; Martins, Â.; Carvalho, A.P. Copper(II) aza-bis(oxazoline) complex immobilized onto ITQ-2 and MCM-22 based materials as heterogeneous catalysts for the cyclopropanation of styrene. *Microporous Mesoporous Mater.* **2013**, *179*, 231–241. [CrossRef]
46. Bolm, C. Vanadium-catalyzed asymmetric oxidations. *Coord. Chem. Rev.* **2003**, *237*, 245–256. [CrossRef]